ICAS-84-3.2.4

RELATIONS BETWEEN MICROSTRUCTURE, MICROTEXTURE AND MECHANICAL PROPERTIES OF PAN-BASE CARBON FIBRES

M. GUIGON
UTC, Departement de Génie Mécanique
60206 COMPIEGNE (FRANCE)

A. OBERLIN
Laboratoire Marcel Mathieu, ER 131 du CNRS
45046 ORLEANS CEDEX (FRANCE)

G. DESARMOT
OFFICE NATIONAL D'ETUDES ET DE RECHERCHES AEROSPATIALES
BP 72 - 92322 CHATILLON CEDEX (FRANCE)

Summary

Some high tensile strength and high modulus PAN-base carbon fibres were studied by TEM :

- HTS fibres are made of aromatic basic structural units (BSU) less than 10Å in size associated edge to edge in parallel to form larger wrinckled aromatic layer sheets. The sheets are crumpled parallel to the fibre axis and then the folds are entangled. This results in a porous texture ; a close-packing index Δ_t is defined and related to the tensile strength to failure σ_c. σ_c increases as Δ_t increases. Values of Young's modulus vary little.

- HM fibres are made of BSU which are almost isometric in shape but folded and parallel to the fibre axis. Their diameters L_a vary from 200 to 700A and the radii of the curvature r_t vary from 20 to 130A. The value of the tensile strength σ_c was found to decrease as $\bar{r}_t/\bar{L}_a$ increased ; Young's modulus and electrical resistivity vary as $1/\bar{L}_a$ does.

I - Introduction

A carbon fibre is a system of aromatic layers, the plane of which is nearly parallel to the fibre axis, that is, the normal c to the layers are nearly perpendicular to the fibre axis. In addition, these aromatic layers are piled up in stacks (basic structural unit or BSU) showing usually a turbostratic structure in which the layers are in complete rotational disorder. The microtexture of a fibre is the BSU arrangement in space. Nevertheless such definition is quite general, the microstructure and microtexture of high strength and high modulus fibres are very different.

In order to describe a fibre, the cristallinity of BSU has to be determined. Their shape, size and distorsion, as well as their relative misorientation and their mutual arrangement in space have to be known. TEM is the only appropriate technique for determining fibre structure from the values of these parameters. As TEM images are two-dimensional projections on the observation plane of all the details contained in the object, it is necessary to use several projections along various directions to restore the features of BSU [1] to [4]. Bright-field, dark-field, 002 lattice-fringe imaging and selected area electron diffraction (SAD) are necessary to determine a structural model for each kind of carbon fibres. The mechanical properties of carbon fibres depend strongly of their microtextural characteristics.

II - Sampling and preparation

After embedding in a suitable medium (epoxy resin), carbon fibres are thin-sectioned by means of an ultramicrotome equipped with a diamond knife, as well in transverse as in longitudinal sections ; fragments are obtained by gentle grinding.

To compare the mechanical properties, single filament tests are performed at the same gauge length, i.e 100 mm for high strength fibres. In the case of high modulus fibres the gauge length is 15 mm and resistivity measurements are presented in addition. The cross section of each filament is measured by electronic scanning microscopy with a well calibrated magnification [5].

III - Results

III-1 - TEM examinations of high strength fibres

III-1-1 - SAD patterns

The reciprocal space of a single aromatic layer is made of sets of hk reciprocal lines perpendicular to the [001] reciprocal plane (Fig. 1 a). The turbostratic structure is made of aromatic layers piled up in parallel but in complete rotational disorder. Hence the reciprocal space of the stacks is made of concentric cylinders generated by the rotation of each set of hk lines (Fig. 1 b) ; the half width of them is L_a^{-1} if L_a is the "diameter" of aromatic layers. 001 nodes along the cylinders axis are due to the stacking of layers. Then, the reciprocal space of a fibre is obtained by rotating Fig. 1 b around fibre axis AA'.

The SAD pattern of a longitudinal section is a plane section cutting the reciprocal space as shown in Fig. 1 c. Since the aromatic layers are misoriented relative to the fibre axis, the cylinders axis CC' generates a cone. The SAD pattern in Fig. 1 d is characteristic of the high strength fibres. Transverse sections patterns are Debye-Scherrer ones as shown in Fig. 2. For all the the samples studied such patterns are obtained : it means that the carbon of the high strength fibres is entirely turbostractic.

III-1-2 - Dark-field and Lattice-fringe imaging

Dark-field and Lattice-fringe imaging are used to determine twist angle β and tilt angle α between stack of aromatic layers. Lattice-fringe imaging gives the spacial arrangement of BSU.

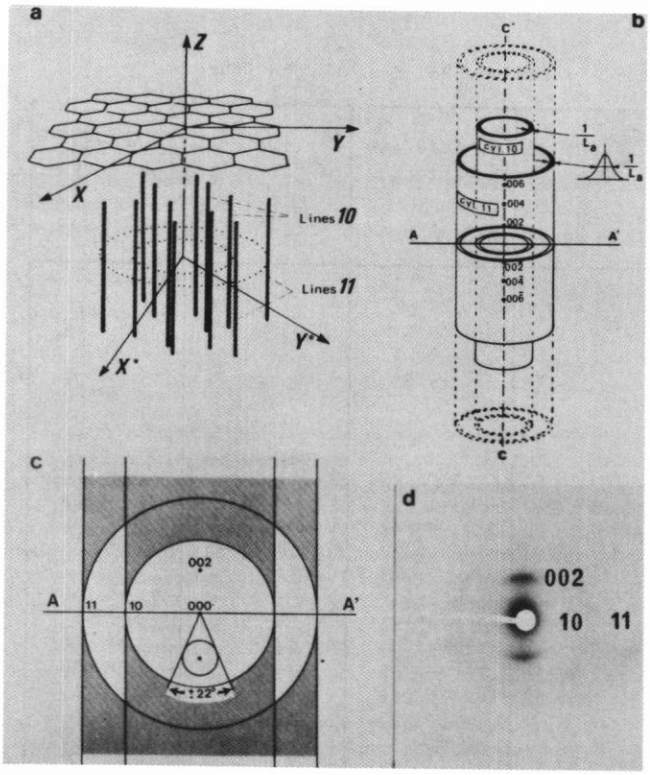

Fig. 1 – (a) Reciprocal space of a single aromatic layer.
(b) Reciprocal space of turbostratic stacks.
(c) Schematic SAD pattern of a fibre (longitudinal section).
(d) SAD pattern of a longitudinal section of Courtaulds XAS, E4 LXA 33B63A.

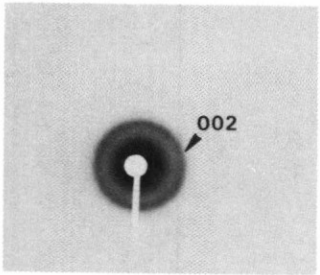

Fig. 2 – SAD pattern of a transverse section of Courtaulds XAS.

II-1-2-1 - Longitudinal sections

All fibres give similar results. Fig. 3 a shows the 002 diffraction image of a longitudinal section : BSU fulfilling Bragg condition are imaged as bright domains less than 10Å in size (L) and are seen edge-on. They are gathered into elongated clusters lengthened along the fibre axis. Inset in fig. 3 a gives a schematic view of clusters. In 002 Lattice-fringe images (Fig. 3 b), small stacks of two or three parallel fringes are observed, see inset in Fig. 3 b. They correspond to the bright domains observed above and correspond to BSU. Tilt angle between BSU is larger than ± 10° ; twist angle is about ± 20°.

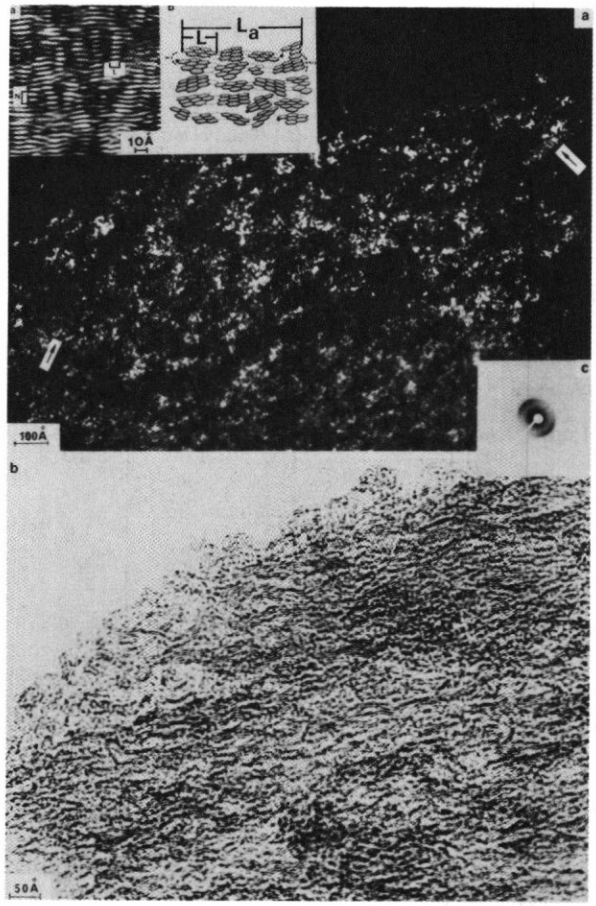

Fig. 3 – (a) 002 dark-field of a longitudinal section of Toray 300, 40B 2600221. Inset c : SAD pattern of the longitudinal section.
(b) 002 lattice fringes of Serofim AXT 2666. Inset b : schematic representation of BSU preferred orientation. Inset a : magnification of a detail to be compared to the inset b.

III-1-2-2 - Transverse sections

Here also all fibres give similar results. Bright domains are observed in dark-field images (Fig. 4 a). Lattice-fringe image (Fig. 4 b) is different of which in Fig. 3 b. Wrinckled layers, made of BSU associated with tilt and twist boundaries, change continuously not only in direction but also in thickness. They can separate into two sheets or more, each sheet being strongly entangled with others. The texture is an open one, though intricate and complex. Nevertheless aromatic layers remain parallel to fibre axis.

It is possible to define an arbitrary index Δ_t called transverse close-packing index which helps to evaluate the packing of the structure. The values of Δ_t take into account the presence of microvoids in it. Δ_t is taken 0.9 for the more compact structure and 0.2 for the more open one (values of $\Delta_t > 0.9$ or < 0.2 are possible for fibres not studied here). All the images are classified between these bounds, see Table I. It must be pointed that the same classification was obtained by two independent observers.

Table I
Mechanical Properties of 16 Samples of High Tensile Strength, PAN-Base Carbon Fibres

Samples	Close packing index Δ_t	Tensile strength σ_c(GPa)	Strain to failure ε_c(%)	Secant Young's E_s(GPa)	Coefficient of variation $CV\sigma_c$(%)	Coefficient of variation $CV\varepsilon_c$(%)	Hetero-geneity
Serofim AXT F15000 3245EY	0.2	1.86	0.85	213	35	27.5	0
Celanese 3000 HTA 7W 7111	0.4	1.67	0.75	223	27	26	frequent
Celanese 1000 HTA 8W 7511	0.4	1.93	0.85	229	30	27	frequent
Celanese 6000 HTA 7 7711	0.5	2.22	0.98	229	18.5	18.5	0
Serofim AXT F15000 4626.15	0.5	2.31	1.11	209	20	20	very frequent
Serofim AXT F15000 2666	0.5	-	-	-	-	-	0
Serofim AXT F15000 4225EY	0.5	-	-	-	-	-	very frequent
Nippon Carbolon Z3/06RBO 9700 5	0.6	2.25	1.04	215	27	16	frequent
Toho HTA7 3000	0.7	2.61	1.14	229	14	13.5	0
Toray T300 90A 014 0562	0.8	-	-	-	-	-	very frequent
Toray T300 40B 16 00 501	0.8	2.22	0.99	225	14	14	frequent
26 00 221	0.8	2.48	1.09	226	21.1	18	frequent
Celanese epoxy JJ 008 HTA 7 0431	0.8	2.54	1.08	236	20.6	20.4	frequent
Courtaulds XAS 6K ILXA 102B 2A	0.8	2.75	1.11	242	9.4	8.5	rare
E4 LXA 33B 63A	0.8	-	-	-	-	-	very frequent
Courtaulds HTS 2T/79 D61/ 79 2	0.9	2.78	1.12	248	18	14.8	0

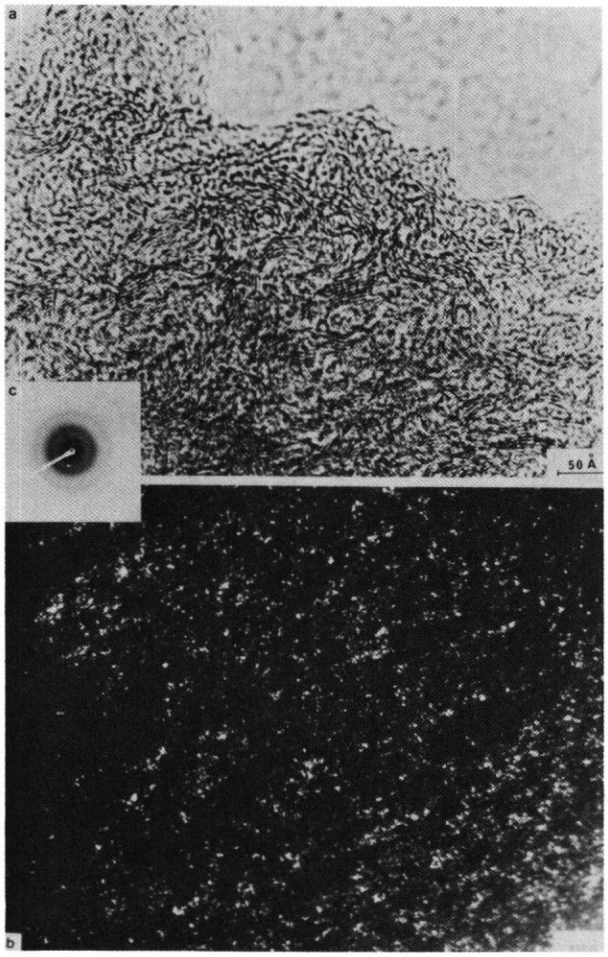

Fig. 4 – (a) 002 lattice fringes of a transverse section of Serofim AXT 2666. (b) 002 dark-field of a transverse section of Toray 300, 40B 2600221. Inset c : SAD pattern.

III-2 - Mechanical properties

Young secant modulus E_s [5], tensile strength σ_c and strain ε_c at failure were measured for each filament. About 16 samples were tested for each type of fibres. In a single filament test, σ_c and ε_c are not characteristic of the material stricto sensu. They are functions of gauge length. However for a given one, we can compare σ_c and ε_c of various carbon fibres. In addition, it should be stated that measurements are local view of mechanical performances related to microscopic examinations performed nearly at the same place in a tow.

IV - Discussion and Conclusion

IV-1 - Model of structure

Fig. 5 a shows a model of a porous carbon which fits well with the microtexture data of all carbonaceous materials in the range 500°C-2000°C. To represent the texture in high strength fibres, this model has to be stretched only along the AA' direction which becomes the AA' axis of the fibre (Fig. 5 b). BSU of about 10A in size are attached in a zigzag thus forming larger wrinckled layers which are crumpled an entangled transversally (D in Fig. 5 b). When two crumpled sheets of layers become close enough, bonding occurs in the faulty areas (cross-linking atoms, tetrahedral bonds, etc at boundaries) which gives lateral cohesion to the fibre.

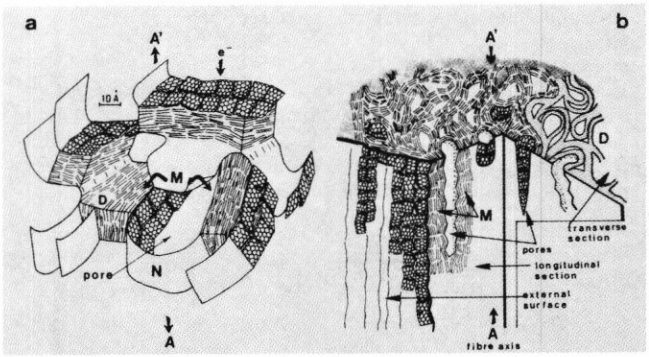

Fig. 5 – Model of:(a) a porous carbon, (b) a high tensile strength fibre derived from (a).

IV-2 - Interpretation of mechanical properties

Fig. 6 shows a linear plot of strength σ_c versus Δ_t (close packing index). TEM data show that ordering in carbon increases from SEROFIM 3245 to COURTAULDS HTS : Δ_t describes this tendency. Simultaneously, the density of lateral bonds between adjacent layers stacks increases. Failure of a filament is mainly due to the propagation of transversal microcracks. In the anisotropic BSU forming the crumpled sheets of carbon layers, a crack can only propagate between layers, impeded by lateral bonds which are stronger than π bonds. Thus σ_c increases with the density of these bonds, i.e with Δ_t . As it can be seen in table 1, the strength distributions become narrow and narrow ($CV\sigma_c$) as Δ_t increases : it is necessary to accumulate a higher number of single breakages to reach a crack of critical size in a more and more compact structure. Because aromatic layers are arranged in flexible zigzags, the moduli E_s are low and nearly constant.

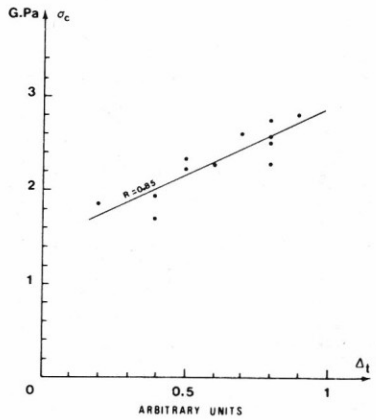

Fig. 6 – $\sigma_c = f(\Delta_t)$.

V - TEM examinations of high modulus fibres

BSU of high modulus fibres are very different of small BSU found for high strength fibres (≈10Å). As shown in Fig. 7 a, a high modulus fibre BSU is a carbon layer stack L_c thick made up of N layers, almost isometric in shape (L_a "diameter"), but bent and rolled around the fibre axis AA'. Bending is characterized first by the transverse radius of curvature r_t and by the extent of the fold. It was found experimentally that the smaller r_t, the more

prominent and the more accentuated the fold. The shape, the size (L_a, L_c, N and r_t) and the mutual arrangement of the BSU can be determined by combining the various mode of imaging and the two possible directions of sectionning (See table II). For instance, 002 Lattice-fringe imaging gives directly r_t ; in Fig. 7 b one can see a schematic SAD pattern also valid for high modulus fibres.

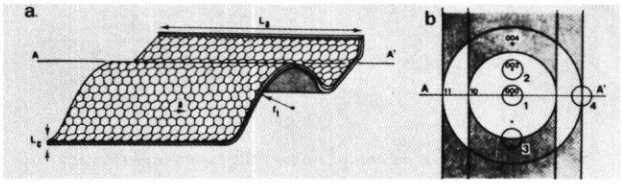

Fig. 7 – (a) Representation of a basic structural unit ; (b) Schematic SAD pattern of a fibre (longitudinal section) with a turbostatic structure.

VI-1 - Longitudinal and transversal sections

Fig. 8 a to 8 d show longitudinal section near the surface of SEROFIM AG58 in bright-field mode and dark-field mode (see Fig. 7 b). A longitudinal section of a fibre contains series of BSU parallel to its axis. In dark-field mode rotational disorder of the stacking induces moiré fringes. Features of moiré (contrast, extention, width of bands...) depend of r_t and are also related to L_c [6] . Fig. 9a is a SAD pattern of the surface region in AG58. Carbon is here partially graphitized with high values for r_t and L_a. High modulus fibres are not "graphite fibres" ! carbon remains turbostratic even in AG58 in which ordering is the highest ; for instance Fig. 9 b shows a SAD pattern of the core region in GY70. In spite of large r_t and L_a (table II), this pattern indicates the turbostratic nature of layers stacks.

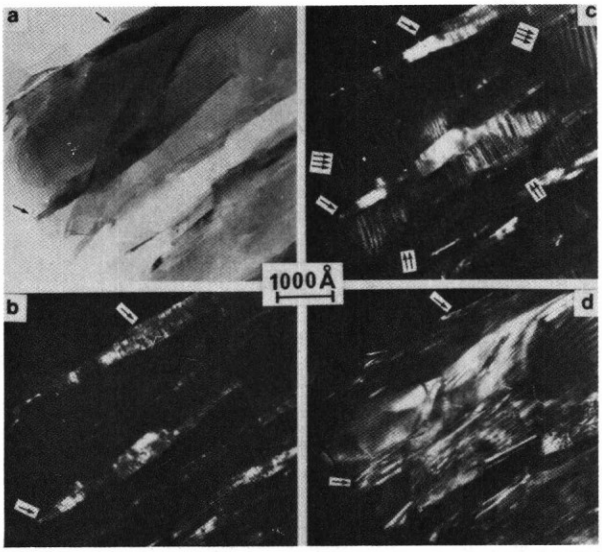

Fig. 8 – Longitudinal section near the fibre surface for Serofim AG58 : (a) BF image (position 1 of Fig. 7b) ; (b) 002 DF image (position 2) ; (c) 10 DF image (position 3) ; (d) 11 DF image (position 4).

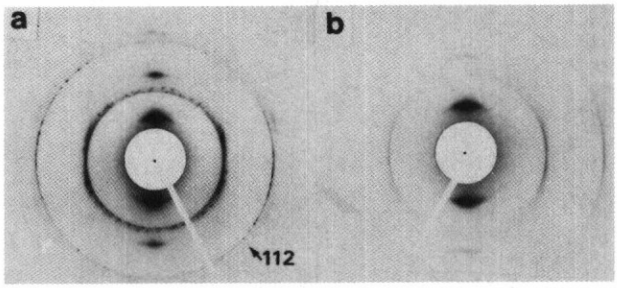

Fig. 9 – SAD patterns of longitudinal sections : (a) surface ofSerofim AG 58 ; (b) Core of Celion GY 70.

Table II
Physical Properties of Various Fibre Samples

Samples	Radius of curvature r_t (Å)	Mean radius of curvature $\bar{r}_t$ (Å)	Tensile strength to failure ρ_c (GPa)	Strain to failure ε_c (%)	Young's modulus E (GPa)	Electrical resistivity ρ ($\mu\Omega$m)	Layer diameter L_a (Å)	Mean layer diameter L_a (Å)
Courtaulds HMS E2M 278 D 82	15-25	23	2.41	0.66	361	8.29	250-500	350
Serofim AG F10000 4212.1	15-25	20	2.41	0.74	326	9.34	200-300	250
Serofim AG F10000 4022.4	25-35	30	2.14	0.67	320	10.04	150-300	250
Serofim AGT F10000 4033.3	25-35	30	-	-	-	-	150-250	230
Serofim AG F1000 0413.11	skin: 60-100 core: 20-30	80 25 35	2.18	0.67	323	9.71	250-350	310
Serofim AG F1000 4022.6	skin: 50-70 core: 30-40	55 35 38	1.67	0.55	304	10.31	150-250	230
Celion GY 70	skin:100-300 core: 50-80	150 60 77	1.53	0.35	430	7.36	skin:450-650 core:300-450	460
Serofim AG 25	skin:200-500 core: 60-100	350 80 130	1.52	0.36	420	5.57	skin:750-900 core:500-750	710

Fig. 10 is an example of longitudinal section, Lattice-fringe mode (SEROFIM AG25, very similar to AG58). L_c corresponds to N = 10 to 20 ; N is of the same order of magnitude for all fibres. Fig. 11 and 12 are Lattice-fringe images of transverse sections (SEROFIM AG58 and COURTAULDS HMS).

In table II samples investigated are presented in increasing order of $\bar{r}_t$, mean value of r_t over the section. Some fibres exhibit skin-core structure. It means that the radius of curvature of BSU varies continuously from the core to the surface but clear boundary is not observed.

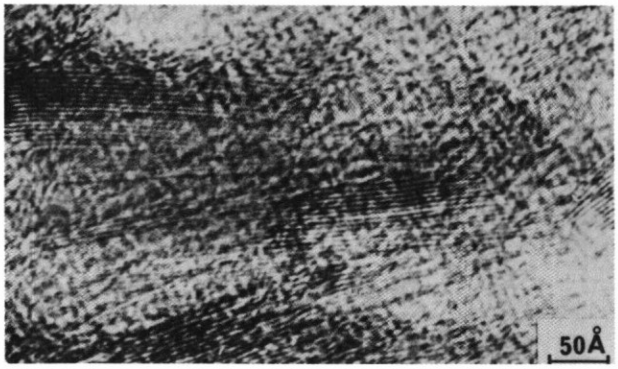

Fig. 10 – Lattice-fringe image of a longitudinal section : surface of Serofim AG 25.

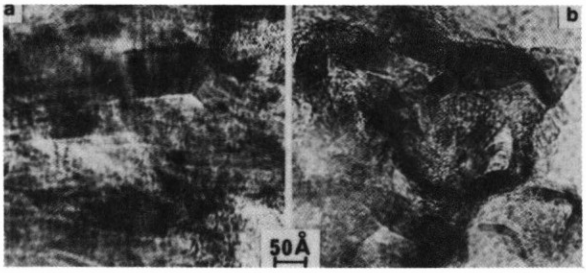

Fig. 11 – Lattice-fringe images of transverse sections of Serofim AG58
a) area near fibre surface ;
b) area near the core.

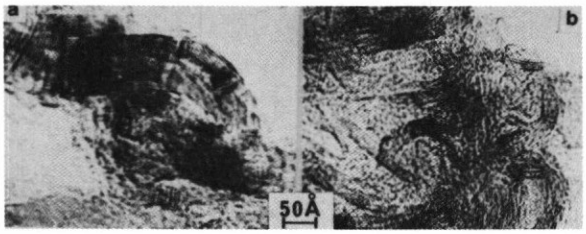

Fig. 11 – Lattice-fringe images of transverse sections of Celion GY 70 :
a) area near fibre surface ;
b) area near the core.

VI - Discussion and conclusion

VI-1 - Model of texture

A model consistent with the preceding results is sketched in fig. 13 beside high strength carbon fibres model. It is similar to very entangled sheets of paper crumpled along the fibre axis. Such a crumpling results in irregular pores elongated parallel to the fibre axis. This model derives directly from that proposed for high strength fibres. The wrinckled layers made of small BSU associated edge to edge are dewrinkled in high modulus fibres. The disappearance of the zigzag structure has already been observed from low-temperature to high temperature carbons (> 2000°C) [7] [8]. From one type of fibre to another, only $\bar{r}_t$ has to be changed and as it decreases, the BSU become increasingly entangled and the fibre is more compact. $\bar{r}_t$ is substituted for the close-packing index Δ_t used as a characteristic parameter for high strenght fibres.

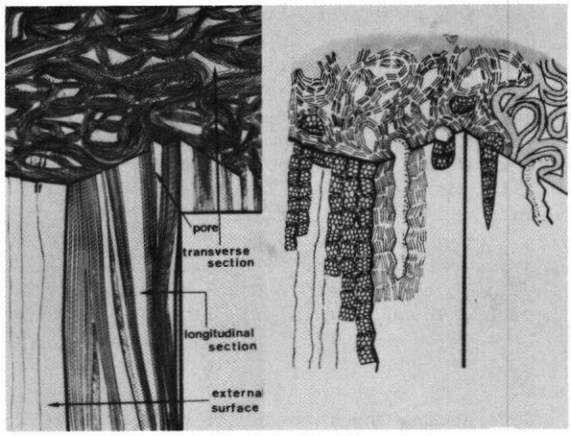

Fig. 13 – Left : high modulus fibre model ; right : high strength fibre model.

VI-2 - Interpretation of mechanical properties

The less ordered fibres (COURTAULDS HMS) are the more severely folded ($\bar{r}_t$ minimum) ; the better ordered one (SEROFIM AG58 and AG25) are the less folded and partially graphitized. Hence r_t increases like ordering, as Δ_t in high strength fibres. However the strength σ_c of high modulus fibres does not appear like a simple function of $\bar{r}_t$ but as a function of $\bar{r}_t/\bar{L}_a$ (Fig. 14). Fibre failure is due to the propagation of transverse microcracks which run freely between aromatic layers ; lateral bonds or tetrahedral bonds tend to impede crack propagation. This impeding effect increases as the density d of these bonds. In high modulus fibres, it was found that the smaller r_t, the more prominent the folds and thus the more entangled they are with others. Correspondingly the larger the number of folds per BSU, the larger the chances of faulty areas to come into contact to establish lateral bonds. The density d of lateral bonds thus depends on the number of folds per BSU, that is, on $\bar{L}_a/\bar{r}_t$. As σ_c is considered to vary with d (i.e $\bar{L}_a/\bar{r}_t$), the best fit is given by :

$$\sigma_c = a - b\frac{\bar{r}_t}{\bar{L}_a} \quad \text{(Fig. 14)}$$

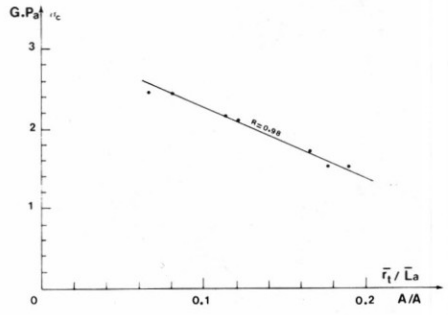

Fig. 14 – $\sigma_c = f(\bar{r}_t/\bar{L}_a)$.

[σ_c should have been written as $\sigma_c = f(d) = f(\bar{L}_a/\bar{r}_t^c)$, but a linear correlation appears when σ_c is expressed as a function of d^{-1} : small values of $\bar{r}_t/\bar{L}_a$, i.e high values of σ_c, correspond to high values of d which is consistent with the assumption made above].

Correlation appears with E, ε_c and ρ : $E = f(\bar{L}_a^{-1})$, $\varepsilon_c = f(\bar{r}_t^{-1})$ and $\rho = f(\bar{L}_a^{-1})$ (Fig. 15, 16). Young modulus varies as the inverse of $\bar{L}_a$: the larger the aromatic layers, the larger the cohesion of the BSU and thus also of the fibre and consequently the larger E. In a compact texture ($\bar{r}_t$ minimum), a greater number of microcracks are needed to obtain catastrophic fracture : this permits a larger elongation. The linear correlation between ρ and $\bar{L}_a^{-1}$ is explained as follows : resistivity increases as the bonds contained in the BSU boundaries perpendicular to the fibre axis do. The surface of these defective areas is proportional to $\bar{L}_a \times \bar{L}_c$. The number of BSU per unit volume is $(\bar{L}_a^2.\bar{L}_c)^{-1}$. The density of defective surface areas is thus $\bar{L}_a^{-1}$. Hence $\rho = f(\bar{L}_a^{-1})$.

Considering the results for high strength fibres, σ_c follows the increase and the decrease of lateral bonding, from the weakest high strength fibres to the more ordered high modulus fibres, passing through a maximum. E is related to the cohesion of the layers.

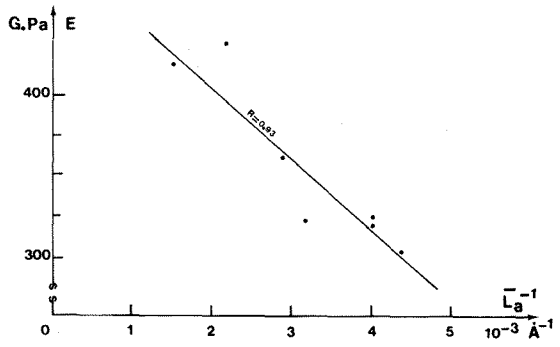

Fig. 15 – $E = f(\bar{L}_a^{-1})$.

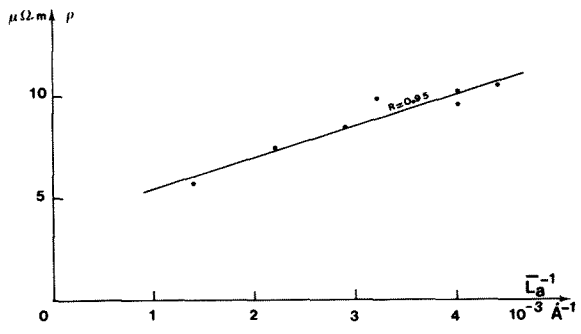

Fig. 16 – $\rho = f(\bar{L}_a^{-1})$.

References

(1) A. OBERLIN, J.L. BOULMIER and B. DURAND, Geochim. Cosmochim. Acta, 38, 1974, 647

(2) A. OBERLIN, M. OBERLIN and M. MAUBOIS, Phil. Mag., 32, 1975, 833

(3) A. OBERLIN, J.L. BOULMIER and M. VILLEY, Kerogen (Ed. B. DURAND), Technip, Paris 1980, 191

(4) A. OBERLIN, J. AYACHE, M. OBERLIN and M. GUIGON , J. Polymer Sci., 20, 1982, 579

(5) G. DESARMOT and M.C. MERIENNE, ONERA Technical Report 4/3551 M, 1982

(6) M. GUIGON , A. OBERLIN, G. DESARMOT, Fibre Science and Technology 20, 1984, 177

(7) A. OBERLIN and G. TERRIERE, J. Microscopy, 18, 1973, 247

(8) J. GOMA and M. OBERLIN, Thin Solid Fibres, 65, 1980, 221